Letter

Asymmetry-induced isolated fully synchronized state in coupled oscillator populations

Oleh E. Omel'chenko [1,*] Jorge Luis Ocampo-Espindola,[2] and István Z. Kiss[2]

[1]*Institute of Physics and Astronomy, University of Potsdam, Karl-Liebknecht-Straße 24/25, 14476 Potsdam, Germany*

[2]*Department of Chemistry, Saint Louis University, 3501 Laclede Avenue, St. Louis, Missouri 63103, USA*

(Received 26 April 2021; accepted 4 July 2021; published 11 August 2021)

A symmetry-breaking mechanism is investigated that creates bistability between fully and partially synchronized states in oscillator networks. Two populations of oscillators with unimodal frequency distribution and different amplitudes, in the presence of weak global coupling, are shown to simplify to a modular network with asymmetrical coupling. With increasing the coupling strength, a synchronization transition is observed with an isolated fully synchronized state. The results are interpreted theoretically in the thermodynamic limit and confirmed in experiments with chemical oscillators.

DOI: 10.1103/PhysRevE.104.L022202

Introduction. Biological and engineered systems often consist of discrete oscillatory units with slightly different properties (e.g., natural amplitudes and frequencies), and coupling among the units can generate collective rhythms that are essential for normal operation [1–4]. Many features of the transition to synchronization can be captured with simplified models, e.g., with the Kuramoto phase model, that predicts "classical" transitions, e.g., second-order phase transitions with continuous increase of order above a critical coupling strength [5,6]. A sudden increase of the order parameter due to first-order transitions can also be observed with an increase in coupling, e.g., for specific natural frequency distributions [7–9], for strongly coupled relaxation oscillators [10], with coupling delays [11] or low-pass filters [12], or with correlations of network properties (degree with natural frequencies) [13–15]; in these examples the order parameter vs the coupling strength curves often exhibit S shapes with two stable and one unstable branches.

All the above synchronization transitions have a common feature: For sufficiently large values of coupling strength they predict approaching the fully synchronized state where all oscillators behave identically. The question naturally arises whether this feature is general or qualitatively different synchronization scenarios could exist. For example, a practically dangerous situation can occur in scenarios where certain states are isolated from other states and thus cannot be obtained from continuation, i.e., through sweeping the coupling strength up and down. Such states often lie on isolas in bifurcation diagrams, where the stable states are created and destroyed through fold bifurcations.

One natural situation where isolas can occur is in networks of oscillators where chimera states (i.e., partially synchronized states of identical phase oscillators in symmetric networks [16]) impede the transition to full synchronization. In this particular case, isolated fully synchronized states were predicted for small parameter regions in phase oscillator models with an explicit two-population coupling [17,18].

In this Letter we show that nonclassical synchronization transitions with an isolated fully synchronized state in general can be found in a population of oscillators that exhibit heterogeneities in both amplitudes and natural frequencies. For this we consider a system of two populations ($\sigma = 1, 2$) of Stuart-Landau oscillators

$$\dot{W}_j^{(\sigma)} = \left(q_\sigma^2 + i\omega_j^{(\sigma)} - \left|W_j^{(\sigma)}\right|^2\right) W_j^{(\sigma)} + Ke^{-i\alpha}(\langle W\rangle - W_j^{(\sigma)}), \quad j = 1, \ldots, N_\sigma, \qquad (1)$$

coupled via their mean field

$$\langle W\rangle = \frac{1}{N_1 + N_2}\left(\sum_{k=1}^{N_1} W_k^{(1)} + \sum_{k=1}^{N_2} W_k^{(2)}\right),$$

with a complex coefficient $Ke^{-i\alpha}$, where $K \in [0, \infty)$ and $\alpha \in (-\pi/2, \pi/2)$ are real parameters referred to as the coupling strength and the phase lag. In the absence of coupling ($K = 0$) each oscillator $W_j^{(\sigma)}(t) \in \mathbb{C}$ has an attracting circular limit cycle of radius $q_\sigma \in (0, \infty)$ along which it rotates with a frequency $\omega_j^{(\sigma)} \in \mathbb{R}$. We assume that the amplitudes q_σ are constant within each of the populations, while the frequencies $\omega_j^{(\sigma)}$ are chosen randomly and independently from Lorentzian distributions

$$g_\sigma(\omega) = \frac{\gamma_\sigma}{\pi}\frac{1}{\omega^2 + \gamma_\sigma^2}, \quad \sigma = 1, 2,$$

with widths $\gamma_\sigma > 0$. In the symmetric case $q_1 = q_2$ the system (1) becomes a single globally coupled population, which was considered in [19]. In contrast, here we focus on the asymmetric case $q_1 \neq q_2$, which occurs if oscillators of two different types are mixed together. Note that such amplitude asymmetry sometimes can emerge spontaneously in globally coupled limit cycle oscillators [20], where it serves as a prerequisite for the symmetry-breaking partially synchronized states called chimera states [20,21].

*Corresponding author: omelchenko@uni-potsdam.de

For simplicity, we consider the weak-coupling case $K \ll 1$. Then the system (1) can be reduced to a phase oscillator model with a type of asymmetrical coupling topology. Using the polar coordinate ansatz

$$W_j^{(\sigma)}(t) = b_j^{(\sigma)}(t) \exp\left[i\theta_j^{(\sigma)}(t)\right],$$

we find that the amplitudes of the oscillators $b_j^{(\sigma)}(t)$ remain almost unchanged, whereas their phases $\theta_j^{(\sigma)}(t)$ evolve according to

$$\dot{\theta}_j^{(\sigma)} = \tilde{\omega}_j^{(\sigma)} + \sum_{\sigma'=1}^{2} \frac{\kappa_{\sigma\sigma'}}{N_{\sigma'}} \sum_{k=1}^{N_{\sigma'}} \sin\left(\theta_k^{(\sigma')} - \theta_j^{(\sigma)} - \alpha\right), \qquad (2)$$

where $\tilde{\omega}_j^{(\sigma)} = \omega_j^{(\sigma)} + K \sin\alpha$ and

$$\kappa_{\sigma\sigma'} = \frac{KN_{\sigma'}}{N_1 + N_2} \frac{q_{\sigma'}}{q_\sigma}. \qquad (3)$$

Equation (3) shows that each oscillator in (2) influences other oscillators with a strength proportional to its amplitude, while the oscillator's sensitivity to the impact of other oscillators is inversely proportional to its amplitude. Note that the two-population models of the form (2) have been studied in many other works [17,18,22–26], but with qualitatively different connectivity matrices $\kappa_{\sigma\sigma'}$. For example, symmetric matrices with positive elements $\kappa_{11} = \kappa_{22} > \kappa_{21} = \kappa_{21}$ have been used in several studies of chimera states [17,18,22]. Moreover, matrices $\kappa_{\sigma\sigma'}$ with positive and negative elements have been considered in [23,24]. Furthermore, connectivity matrices of the form $\kappa_{\sigma\sigma'} \sim d_\sigma d_{\sigma'}$, where d_σ denotes the node degree, were related to the annealed approximation of random Kuramoto networks [25,26]. However, it is easy to see that the connectivity matrix (3) cannot be reduced to any of the above examples.

In the following we assume that the population sizes are equal, $N_1 = N_2$. Without loss of generality, we choose $q_2 > q_1$; then the small-amplitude oscillators and the large-amplitude oscillators are grouped into the first and second populations, respectively. Defining the amplitude ratio $\mu = q_2/q_1$ and inserting this into Eq. (3), we obtain the expressions for the connectivity matrix $\kappa_{\sigma\sigma'}$,

$$\kappa_{11} = \kappa_{22} = \frac{K}{2}, \quad \kappa_{12} = \frac{K\mu}{2}, \quad \kappa_{21} = \frac{K}{2\mu}, \qquad (4)$$

illustrated schematically in Fig. 1(a). Note that the amplitude ratio μ also acts as an interpopulation coupling asymmetry factor.

Thermodynamic limit analysis. In the thermodynamic limit $N_1 = N_2 \to \infty$, the state of the system (2) can be described by the probability density function $f_\sigma(\omega, \theta, t)$ for each population σ; then

$$z_\sigma(t) = \int_{-\infty}^{\infty} d\omega \int_0^{2\pi} f_\sigma(\omega, \theta, t) e^{i\theta} d\theta \qquad (5)$$

is the complex order parameter of the σth population. The modulus of z_σ satisfies $|z_\sigma(t)| \in [0, 1]$ and measures the synchrony of the σth population. Small values of $|z_\sigma(t)|$ correspond to asynchronous population dynamics, while $|z_\sigma(t)| = 1$ indicates its perfect synchrony. Using a standard analytical procedure (see Sec. 3.1.1 in [27]), we can show that

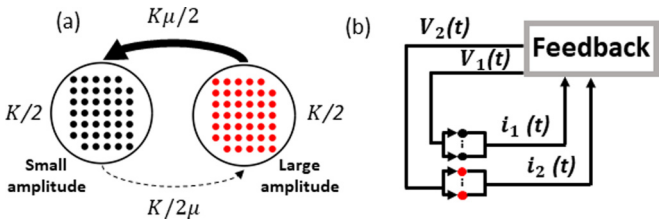

FIG. 1. Network schematic and experimental setup. (a) Schematic of the network topology exhibiting the same intrapopulation but differing interpopulation coupling strength. (b) Experimental implementation of the feedback scheme. The currents of each population are measured $[i_k(t)]$ and fed back to the applied circuit potentials (V_k) according to Eqs. (11) and (12). Each population has 40 electrodes (only two are shown for clarity).

the long-term dynamics of probability densities f_σ typically settles down on the Ott-Antonsen invariant manifold [28]. The evolution on this manifold is described by a system of two complex ordinary differential equations (ODEs) for z_1 and z_2, which, using the polar coordinate representation $z_\sigma(t) = r_\sigma(t)\exp[i\phi_\sigma(t)]$ and defining $\psi(t) = \phi_2(t) - \phi_1(t)$, can be written as an equivalent real ODE system

$$\dot{r}_1 = -\gamma_1 r_1 + \frac{1 - r_1^2}{2}[\kappa_{11} r_1 \cos\alpha + \kappa_{12} r_2 \cos(\psi - \alpha)], \qquad (6)$$

$$\dot{r}_2 = -\gamma_2 r_2 + \frac{1 - r_2^2}{2}[\kappa_{22} r_2 \cos\alpha + \kappa_{21} r_1 \cos(\psi + \alpha)], \qquad (7)$$

$$\dot{\psi} = \frac{r_1^2 + 1}{2r_1}[\kappa_{11} r_1 \sin\alpha - \kappa_{12} r_2 \sin(\psi - \alpha)] - \frac{r_2^2 + 1}{2r_2}[\kappa_{22} r_2 \sin\alpha + \kappa_{21} r_1 \sin(\psi + \alpha)]. \qquad (8)$$

Below we consider two cases of the system (6)–(8) with the connectivity coefficients $\kappa_{\sigma\sigma'}$ determined by (4): (i) oscillators with identical frequencies $\gamma_1 = \gamma_2 = 0$ and (ii) oscillators with unimodal frequency distribution and identical widths in the two populations $\gamma_1 = \gamma_2 > 0$.

Note that because of (4) the system (6)–(8) with $\gamma_1 = \gamma_2$ is not $\mathbb{Z}_2$ symmetric with respect to the transformation $(r_1, r_2, \psi) \mapsto (r_2, r_1, -\psi)$. This fact makes it qualitatively different from the phase oscillator model considered in [17,18].

Case (i). We start with the case of oscillators with identical frequencies ($\gamma_1 = \gamma_2 = 0$). It is known [29,30] that in this case, the Ott-Antonsen manifold is not attractive and many other dynamical regimes (which are typically quasiperiodic) can be found outside the manifold at different distances from it. On the other hand, all linearly stable equilibria and periodic orbits found in the system (6)–(8) with $\gamma_1 = \gamma_2 = 0$ usually become attractors of the same system for arbitrarily small but positive values of γ_1 and γ_2. Therefore, considering the case $\gamma_1 = \gamma_2 = 0$, we obtain useful information about the behavior of the system (6)–(8) in the singular limit $\gamma_1 = \gamma_2 \to 0$.

Simple calculations demonstrate that the system (6)–(8) with $\gamma_1 = \gamma_2 = 0$ has two types of fixed points. The first type includes fixed points describing fully synchronized states, where each population is synchronized $r_1 = r_2 = 1$ but with a

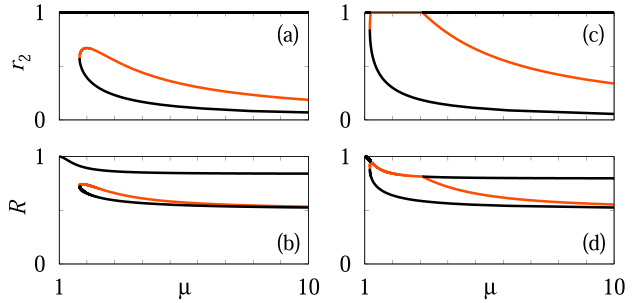

FIG. 2. Stable (black) and unstable [orange (gray)] fixed points of the network (6)–(8) with identical oscillator frequencies ($\gamma_1 = \gamma_2 = 0$) and (a) and (b) $\alpha = 1.15$ and (c) and (d) $\alpha = 1.3$. (a) and (c) Dependence of the second population order parameter r_2 versus the amplitudes ratio μ (for the first population $r_1 = 1$). (b) and (d) Corresponding global order parameters R [see (9)]. Notice that unphysical fixed points $r_2 > 1$ are discarded in (d).

phase shift between their collective phases

$$\psi = \arctan\left(\frac{\mu^2 - 1}{\mu^2 + 1}\tan\alpha\right).$$

The second type includes partially synchronized fixed points with one population fully ($r_1 = 1$) and the second population partially ($r_2 < 1$) synchronized. These points are defined parametrically by the formulas

$$r_2 = -\frac{\cos(\psi + \alpha)}{\mu\cos\alpha},$$

$$\mu^2 = -\frac{\cos^2(\psi + \alpha)\sin\psi/\cos\alpha}{\sin(\psi + 2\alpha)\cos\alpha + 2\cos^2(\psi + \alpha)\sin(\psi - \alpha)},$$

with ψ and α varying in the intervals $[-\pi, \pi]$ and $(-\pi/2, \pi/2)$, respectively. Note that not all values of ψ and α are admissible. First, the expression for r_2 must satisfy the inequality $0 < r_2 \leqslant 1$. Second, the right-hand side of the formula for μ^2 must be positive. Using these restrictions, we find two critical values $\alpha_1 \approx 1.05$ and $\alpha_2 \approx 1.23$ such that for $0 \leqslant \alpha < \alpha_1$ the system (6)–(8) has only the fully synchronized fixed point $r_1 = r_2 = 1$, while for $\alpha > \alpha_1$ and sufficiently large μ it also has two other partially synchronized fixed points (one stable and one unstable) lying on a folded branch. Moreover, for $\alpha > \alpha_2$ there is a bounded interval of μ values where the upper part of the folded branch becomes unphysical ($r_2 > 1$). Figures 2(a) and 2(c) show the two types of fixed points (r_2 vs μ) for two representative values α and Figs. 2(b) and 2(d) show the corresponding global order parameter

$$R = \tfrac{1}{2}|z_1 + z_2| = \tfrac{1}{2}|r_1 + r_2 e^{i\psi}|. \tag{9}$$

[The unphysical branch ($r_2 > 1$) connecting two transcritical bifurcation points is not shown in Fig. 2(d).]

Case (ii). For oscillators with unimodal frequency distribution ($\gamma_1 = \gamma_2 > 0$), without cross coupling the two populations would exhibit a Kuramoto transition to synchrony at the same critical coupling strength. Therefore, symmetry-broken partially synchronized states are due to the cross coupling between the populations. In this case, the dynamics on the Ott-Antonsen manifold

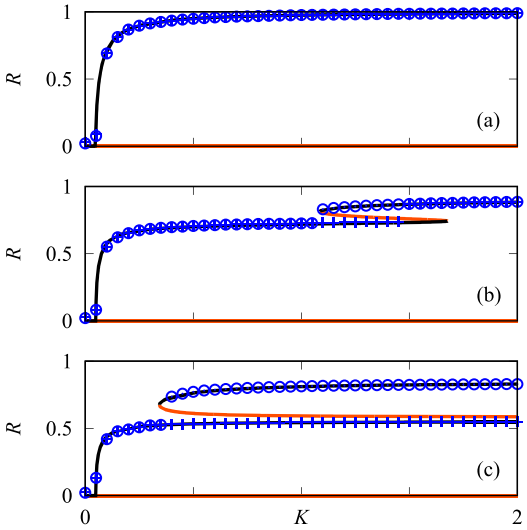

FIG. 3. Synchronization transitions in the network model (6)–(8) with unimodal distribution of the natural frequencies ($\gamma_1 = \gamma_2 = 0.01$) at three different amplitude ratios μ: (a) $\mu = 1$, (b) $\mu = 1.67$, and (c) $\mu = 5$. Stable and unstable branches are shown as black and orange (gray) curves, respectively. The order parameter R is computed by (9). Pluses and circles show the time-averaged global order parameters R_N obtained in the forward and the backward K sweeps (with initial conditions from the previous integration), respectively, for the system (2) with $N_1 = N_2 = 500$ and $\alpha = 1.15$.

[Eqs. (6)–(8)] is relevant to the long-term dynamics of the phase model (2) with heterogeneous natural frequencies $\omega_j^{(\sigma)}$.

The synchronization transitions can be described by the changes of the global order parameter

$$R_N(t) = \frac{1}{N_1 + N_2}\left|\sum_{\sigma=1}^{2}\sum_{k=1}^{N_\sigma} e^{i\theta_k^{(\sigma)}(t)}\right| \tag{10}$$

for the coupling strength K. In the thermodynamic limit $R_N(t) \approx R$ [see (9)]; therefore, the transitions can be predicted by Eqs. (6)–(8). For this we fix values of $\gamma_1 = \gamma_2$, μ, and α, vary the coupling strength K, and compute the corresponding fixed points (r_1, r_2, ψ) of the system (6)–(8) using the Newton-Raphson method. Then inserting the result into (9), we obtain the graph of R versus K. Figure 3 shows qualitatively different synchronization transition scenarios found for $\gamma_1 = \gamma_2 = 0.01$, $\alpha = 1.15$, and several μ. For identical amplitudes in both populations (symmetrical coupling, $\mu = 1$) we recover the well-known classical (second-order) monotonic synchronization transition typical for the Kuramoto model with all-to-all coupling [5,6]. For $\mu = 1.67$ the (nearly) fully synchronized state is reached through an S-shaped (first-order) transition from the partially synchronized state [Fig. 3(b)]. Finally, for $\mu = 5$ [Fig. 3(c)], with increasing the coupling strength, first a partially synchronized state occurs, which retains its stability in the limit of strong (infinite, in the phase model) K. Thus, the (nearly) fully synchronized state is isolated. The corresponding branch starts from a fold bifurcation at a finite coupling strength and ends in the infinite coupling strength limit. The predictions of

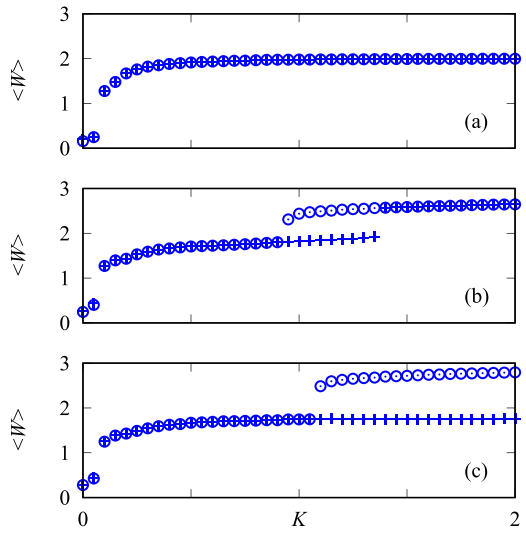

FIG. 4. Synchronization transitions in the system of mean-field coupled Stuart-Landau oscillators (1) with unimodal distribution of the natural frequencies ($\gamma_1 = \gamma_2 = 0.01$) at three different amplitude ratios $\mu = q_2/q_1$: (a) $\mu = 1$, (b) $\mu = 1.8$, and (c) $\mu = 2$. Pluses and circles show the time-averaged mean-field $\langle W \rangle$ obtained in the forward and the backward K sweeps (with initial conditions from the previous integration), respectively. The other parameters are $N_1 = N_2 = 50$, $\alpha = 1.15$, and $q_1 = 2$.

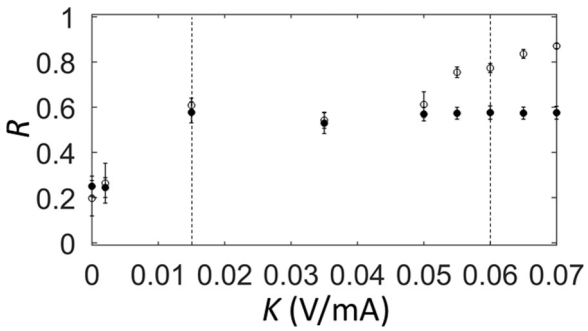

FIG. 5. Synchronization transition in a population of oscillatory chemical reactions. The global order parameter is plotted as a function of the coupling strength. Error bars show the standard deviation of R in the time series for each point. The empty and filled circles correspond to in-phase and random initial conditions, respectively. The states of each population are shown in Fig. 6, marked with the dashed lines.

these nonclassical bifurcation diagrams were confirmed with numerical simulations with $N_1 = N_2 = 500$ oscillators with forward and backward sweeps of the coupling strengths in Fig. 3 (pluses and circles, respectively).

Note that all synchronization transitions described above have an important scaling property. For fixed μ and α, the value of an equilibrium of the system (6)–(8) depends on the ratio K/γ, but not on K and γ separately. This means that every qualitative feature of the synchronization transitions in the system (6)–(8) can be realized for arbitrarily small values K, provided the values of γ_1 and γ_2 are small enough. For example, Fig. 4 shows that every type of synchronization transition from Fig. 3 indeed can be found in the original system of the mean-field coupled Stuart-Landau oscillators (1).

Experiments with electrochemical oscillators. The asymmetry-induced synchronization bistability was explored with 80 electrochemical oscillators (using Ni electrodissolution) that can be coupled with a delayed feedback [31]. At constant circuit potential V, the oscillatory dissolution rate, the corrosion current, of each of the 1-mm-diam nickel wires can be measured in a 3 mol/L sulfuric acid electrolyte maintained at a temperature of 10 °C. It was expected that the theoretically predicted synchronization features can be observed in the experiments, provided the modular network with the asymmetrical coupling between the two groups can be realized.

The first and second populations of 40 wires were connected to the corresponding channels of a bipotentiostat [see Fig. 1(b) for a schematic of the experiments]. The bipotentiostat measured the total currents of each population [$i_1(t)$ and $i_2(t)$] and applied small adjustments of the circuit potentials [$V_1(t)$ and $V_2(t)$] of the two populations

$$V_1(t) = V_0 + K[\tilde{i}_1(t-\tau) + \epsilon_1 \tilde{i}_2(t-\tau)], \tag{11}$$

$$V_2(t) = V_0 + K[\tilde{i}_2(t-\tau) + \epsilon_2 \tilde{i}_1(t-\tau)], \tag{12}$$

where $\tilde{i}_k(t) = i_k(t) - o_k$ is the offset [$o_k(t)$] corrected population current, V_0 is the base circuit potential (at which the oscillations occur), ϵ_1 and ϵ_2 represent the interpopulation coupling factors, K is the feedback gain, which is equivalent to the (overall) coupling strength, and τ is the feedback delay, which corresponds to the phase lag parameter α. According to our previous study [31], the $\alpha/2\pi$ quantity is approximately equal to τ/T_0, where $T_0 = 2.4$ s is the mean period of the uncoupled population ($K = 0$ V/mA). We have chosen $\tau = 0.9T_0/4$, which translates to $\alpha \approx 1.4$ in the theory.

In the experiments, we chose $\epsilon_1 = 0.2$ and $\epsilon_2 = 5.0$, which correspond to asymmetrically coupled populations with $\mu = 5$. A series of experiments was performed with a given coupling strength K, starting from random and in-phase synchronized initial conditions; the mean Kuramoto (global) order parameters for both initial conditions are shown in Fig. 5. For weak coupling ($K < 0.010$ V/mA), a desynchronized state was observed for both initial conditions. For $0.015\ \text{V/mA} \leqslant K \leqslant 0.050\ \text{V/mA}$, the system exhibited the same partially synchronized state for both in-phase and random initial conditions. For $K = 0.015$ V/mA, the Kuramoto order for each population (top), the current oscillations of every element (middle), and the snapshot of the phases (bottom) are shown in Fig. 6(a). Population 1 exhibited a synchronized state, while population 2 was desynchronized.

As it is shown in Fig. 5, with a further increase in the coupling strength ($0.055\ \text{V/mA} \leqslant K \leqslant 0.070$ V/mA), the experiments with in-phase initial conditions resulted in a strongly synchronized state with large Kuramoto order parameter ($R \approx 0.7$–0.8), which differed from a lower synchrony state ($R \approx 0.6$) obtained from desynchronized initial conditions; therefore, bistability was observed. Figure 6(b) shows that the state obtained from the desynchronized initial

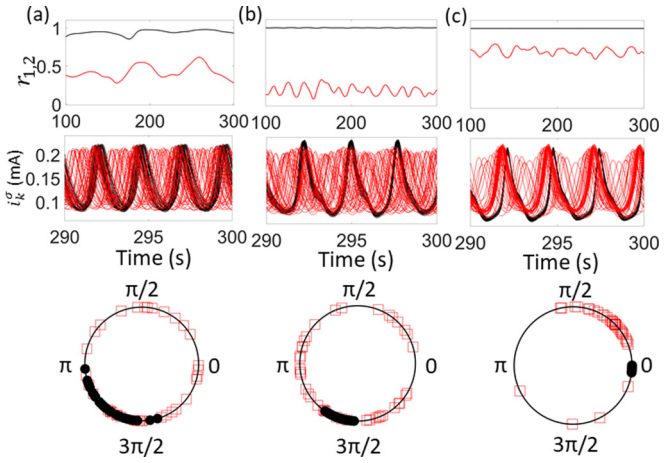

FIG. 6. Multistability of synchronized states observed for different initial conditions in two populations of oscillatory chemical reactions. The black and red lines correspond to populations 1 and 2, respectively. (a) Partially synchronized state with $K = 0.015$ V/mA and in-phase initial conditions. (b) Partially synchronized state with $K = 0.060$ V/mA and random initial conditions. (c) Nearly fully synchronized state with $K = 0.060$ V/mA and in-phase initial conditions. The top row shows the order parameters for each population vs time. The middle row shows the time series of the oscillator currents for each population. The bottom row shows snapshots of the phases (filled circles are for population 1 and empty squares for population 2).

condition for $K = 0.060$ V/mA was similar to the partially synchronized state at lower coupling strength: Population 1 was synchronized and population 2 was desynchronized. However, starting from an in-phase initial condition, we obtained a state where population 2 became partially synchronized [while population 1 remained fully synchronized; see Fig. 6(c)]. The experiments thus showed that the asymmetry-induced bistability in the synchronization pattern is a robust phenomenon, and the comparison of the theoretically predicted [Fig. 3(c)] and experimentally measured (Fig. 5) R vs K graphs indicate the presence of the isolated (nearly) fully synchronized state.

Conclusion. We have shown that a system of globally coupled oscillators, which is a mixture of two populations with different amplitudes, can be reduced in the weak-coupling case to an asymmetrically coupled modular network. The system exhibits nonclassical synchronization transitions, where a partially synchronized state and an isolated (nearly) fully synchronized state coexist for arbitrarily large coupling strength. The experiments demonstrated that the salient dynamical features of the behavior can be observed in systems without amplitude heterogeneity, but with asymmetrical coupling (through parameter μ). Important future directions include exploring the correlations between amplitude heterogeneities and frequency distributions on the observed partially synchronized states, because in experimental settings changing the amplitudes through bifurcation parameters could also impact the frequency distribution.

The predicted synchronization bistability is very robust to finite-size effects as it was observed even with 40 oscillator populations in experiments. In contrast, similar bistable synchronization transitions in coupled oscillator models with nonidentical frequencies but with identical oscillator amplitudes required much larger system sizes (e.g., 10 000 oscillators) for their observation [8,9]. Moreover, it seems likely that finite-size effects were also more pronounced in the bistable synchronization transitions found in other mean-field coupled oscillator models [32–36]. In a more general context, our results show that even relatively small asymmetry in the coupling topology (e.g., through amplitude heterogeneity) can produce very robust partially synchronized states where one population is strongly synchronized while the other is desynchronized. The proposed mechanism thus should be considered for interpretation of partially synchronized states that seem to prevalent in biological systems [37,38], in particular, in various aspects of brain dynamics [39–41].

Acknowledgments. The work of O.E.O. was supported by the Deutsche Forschungsgemeinschaft through Grant No. OM 99/2-1. J.L.O.-E. acknowledges financial support from CONACYT. I.Z.K. acknowledges support from the National Science Foundation through Grant No. CHE-1900011.

[1] A. Winfree, *The Geometry of Biological Time* (Springer, Berlin, 2001).
[2] Y. Kuramoto, *Chemical Oscillations, Waves, and Turbulence* (Springer, Berlin, 1984).
[3] A. Pikovsky, M. Rosenblum, and J. Kurths, *Synchronization: A Universal Concept in Nonlinear Sciences* (Cambridge University Press, Cambridge, 2001).
[4] S. Boccaletti, *Synchronized Dynamics of Complex Systems* (Elsevier Science, Amsterdam, 2008).
[5] S. H. Strogatz, Physica D **143**, 1 (2000).
[6] J. A. Acerbrón, L. L. Bonilla, C. J. Pérez-Vicente, F. Ritort, and R. Spigler, Rev. Mod. Phys. **77**, 137 (2005).
[7] D. Pazó, Phys. Rev. E **72**, 046211 (2005).
[8] O. E. Omel'chenko and M. Wolfrum, Phys. Rev. Lett. **109**, 164101 (2012).
[9] O. E. Omel'chenko and M. Wolfrum, Physica D **263**, 74 (2013).
[10] D. Calugaru, J. F. Totz, E. A. Martens, and H. Engel, Sci. Adv. **6**, eabb2637 (2020).
[11] M. K. Stephen Yeung and S. H. Strogatz, Phys. Rev. Lett. **82**, 648 (1999).
[12] W. Zou, M. Zhan, and J. Kurths, Phys. Rev. E **100**, 012209 (2019).
[13] J. Gómez-Gardeñes, S. Gómez, A. Arenas, and Y. Moreno, Phys. Rev. Lett. **106**, 128701 (2011).
[14] J. G. Restrepo and E. Ott, Europhys. Lett. **107**, 60006 (2014).
[15] F. A. Rodriguez, T. K. D. M. Peron, P. Ji, and J. Kurths, Phys. Rep. **610**, 1 (2016).
[16] M. J. Panaggio and D. M. Abrams, Nonlinearity **28**, R67 (2015).
[17] D. M. Abrams, R. Mirollo, S. H. Strogatz, and D. A. Wiley, Phys. Rev. Lett. **101**, 084103 (2008).
[18] C. R. Laing, Chaos **19**, 013113 (2009).

[19] P. C. Matthews, R. E. Mirollo, and S. H. Strogatz, Physica D **52**, 293 (1991).
[20] L. Schmidt and K. Krischer, Phys. Rev. Lett. **114**, 034101 (2015).
[21] G. C. Sethia and A. Sen, Phys. Rev. Lett. **112**, 144101 (2014).
[22] C. R. Laing, Phys. Rev. E **81**, 066221 (2010).
[23] H. Hong and S. H. Strogatz, Phys. Rev. Lett. **106**, 054102 (2011).
[24] Y. Maistrenko, B. Penkovsky, and M. Rosenblum, Phys. Rev. E **89**, 060901(R) (2014).
[25] S. N. Dorogovtsev, A. V. Goltsev, and J. F. F. Mendes, Rev. Mod. Phys. **80**, 1275 (2008).
[26] D. Iatsenko, P. V. E. McClintock, and A. Stefanovska, Nat. Commun. **5**, 4118 (2014).
[27] C. Bick, M. Goodfellow, C. R. Laing, and E. A. Martens, J. Math. Neurosci. **10**, 9 (2020).
[28] E. Ott and T. M. Antonsen, Chaos **18**, 037113 (2008).
[29] A. Pikovsky and M. Rosenblum, Phys. Rev. Lett. **101**, 264103 (2008).
[30] J. R. Engelbrecht and R. Mirollo, Phys. Rev. Res. **2**, 023057 (2020).
[31] H. Kori, C. G. Rusin, I. Z. Kiss, and J. L. Hudson, Chaos **18**, 026111 (2008).
[32] M. C. Cross, A. Zumdieck, R. Lifshitz, and J. L. Rogers, Phys. Rev. Lett. **93**, 224101 (2004).
[33] L. F. Lafuerza, P. Colet, and R. Toral, Phys. Rev. Lett. **105**, 084101 (2010).
[34] E. Montbrió and D. Pazó, Phys. Rev. Lett. **106**, 254101 (2011).
[35] D. Iatsenko, S. Petkoski, P. V. E. McClintock, and A. Stefanovska, Phys. Rev. Lett. **110**, 064101 (2013).
[36] R. Gallego, E. Montbrió, and D. Pazó, Phys. Rev. E **96**, 042208 (2017).
[37] L. Glass, Nature (London) **410**, 277 (2001).
[38] S. Yamaguchi, H. Isejima, T. Matsuo, R. Okura, K. Yagita, M. Kobayashi, and H. Okamura, Science **302**, 1408 (2003).
[39] P. J. Uhlhaas and W. Singer, Neuron **52**, 155 (2006).
[40] K. Lehnertz, S. Bialonski, M. T. Horstmann, D. Krug, A. Rothkegel, M. Staniek, and T. Wagner, J. Neurosci. Methods **183**, 42 (2009).
[41] P. A. Tass, *Phase Resetting in Medicine and Biology* (Springer, Berlin, 1999).